NEUTRONICS INTEGRAL EXPERIMENTS OF LITHIUM-OXIDE FUSION BLANKET WITH HETEROGENEOUS CONFIGURATIONS USING DEUTERIUM-TRITIUM NEUTRONS

BLANKET ENGINEERING

KEYWORDS: *neutronics experiment, tritium breeding, heterogeneous configuration*

YUKIO OYAMA, CHIKARA KONNO, YUJIRO IKEDA, SEIYA YAMAGUCHI, KOICHI TSUDA, KAZUAKI KOSAKO, HIROSHI MAEKAWA, MASAYUKI NAKAGAWA, TAKAMASA MORI, and TOMOO NAKAMURA
Japan Atomic Energy Research Institute, Department of Reactor Engineering Tokai Research Establishment, Tokai-mura, Naka-gun, Ibaraki-ken 319-11 Japan

MOHAMED A. ABDOU *University of California, Los Angeles School of Engineering and Applied Science Mechanical, Aerospace, and Nuclear Engineering Department Los Angeles, California 90095*

EDGAR F. BENNETT *Argonne National Laboratory, Fusion Power Program Building 205, 9700 South Cass Avenue, Argonne, Illinois 60439*

ANIL KUMAR and MAHMOUD Z. YOUSSEF
University of California, Los Angeles, School of Engineering and Applied Science Mechanical, Aerospace, and Nuclear Engineering Department Los Angeles, California 90095

KARL G. PORGES *Argonne National Laboratory, Fusion Power Program Building 205, 9700 South Cass Avenue, Argonne, Illinois 60439*

Received January 28, 1994
Accepted for Publication July 28, 1994

Neutronics experiments for two types of heterogeneous blankets are performed in the Phase-IIC experiments of the Japan Atomic Energy Research Institute/U.S. Department of Energy collaborative program on fusion blanket neutronics. The experimental system uses the same geometry as the previous Phase-IIA series, which was a closed geometry that used a neutron source enclosure of lithium carbonate. The heterogeneities selected for testing are the beryllium edge-on and the water coolant channel assemblies that appear in typical blankets. In the former, the beryllium and the lithium-oxide (Li_2O) layers are piled up alternately in the front part of the test blanket. In the latter, the two simulated water cooling channels are emplaced vertically in the Li_2O blanket. These channels produce a steep gradient of neutron flux and a significant spectrum change around the material boundary. The calculation accuracy and measurement method for these transient regions are key areas of interest in the experiments. The measurements are performed for the tritium production rate and the other nuclear parameters as well as the previous experiments. The void effect is found to not be negligible around the heterogeneous region for the detector with a low-energy response. At the same time, enhancements of tritium production are seen near the beryllium and hydrogenous material. However, the current Monte Carlo calculation shows good agreement with the experiment even in such a boundary.

I. INTRODUCTION

The tritium breeding blanket in a deuterium-tritium (D-T)–fueled fusion tokamak reactor is composed of various components, e.g., a tritium breeder made of a material containing lithium, a neutron multiplier, structure materials, a tritium gas purging system, and water cooling channels. The neutronic characteristics of the materials used in these components are quite different from each other. For example, lithium largely absorbs low-energy neutrons below several hundred kilo-electron-volts by a $^6Li(n,\alpha)$ reaction while a neutron multiplier such as beryllium supplies low-energy neutrons below 2 MeV by a $^9Be(n,2n)$ reaction. Hence, the heterogeneous arrangement of the blanket components causes large changes in the energy spectrum and the neutron flux around the material boundaries.

In fusion reactor design research, because of the difficulty in making a precise, detailed model for the complicated blanket components, the calculation is usually carried out by homogenizing or approximating the heterogeneous arrangement. However, this is not always a reasonable way to calculate the nuclear parameters that require high accuracy such as the tritium breeding ratio (TBR). Although the Monte Carlo method can be used for the accurate geometry, there remains a statistical problem with estimating the localized parameters at small regions in a large-scale system. This is a major concern when the local parameters are calculated at the transient region in the heterogeneous systems. Thus, a benchmark experiment for heterogeneous systems is required for validation of the applicability of the neutron transport codes and the nuclear data used in the reactor designs.

One type of experiment of the Phase-II experiments of the Japan Atomic Energy Research Institute (JAERI)/U.S. Department of Energy (U.S. DOE) collaborative program on fusion blanket neutronics[1-3] was the neutronics experiments on heterogeneous test blankets that were performed at the JAERI Fusion Neutronics Source (FNS) facility. Two types of heterogeneous blanket systems were tested: the beryllium multilayered [beryllium edge-on (BEO)] system and the water coolant channel (WCC) system.

The BEO system was chosen to make a closer simulation for the mixed system of beryllium and lithium oxide (Li_2O). The preanalysis of the experimental arrangement with an even fraction of beryllium and Li_2O showed that the total tritium production of the BEO system rapidly approaches that of the homogeneously mixed system with an increase in the division of the number of layers when the ratio of the volume of beryllium to that of Li_2O is kept the same in the mixed system. Hence, one can consider that the mixed system consisting of 50-mm layers of each material represents global characteristics of the homogenized system. However, locally, a large transition in the neutron spectrum is still expected at the boundary between the beryllium and the Li_2O.

Another typical case of heterogeneity in a reactor blanket is the WCC system. Because neutrons slow down in the coolant by collision with hydrogen in water, i.e., polyethylene, the tritium production reaction rate greatly increases at the boundary. Then, the $^6Li(n,\alpha)$ reaction produces local peaks of nuclear heating around the coolant channels and affects the TBR. This information is important for the thermohydromechanical design and the tritium recovery system in the blanket.

To provide the experimental data in heterogeneous configurations of blankets for testing the design codes and the database, for the foregoing two heterogeneous test blankets, we performed measurements of the tritium production rate (TPR) and the other nuclear parameters. The results obtained are compared with the homogeneous reference blanket, and the experimental problems relevant to the heterogeneity are discussed together with the result by a transport calculation. The benchmarks of different codes and nuclear data are also performed and discussed separately.[4,5]

II. EXPERIMENTAL SETUP

II.A. Neutron Source Facility

The experiments were performed at the JAERI FNS facility. A rotating tritiated target was used to produce neutrons by $^3T(d,n)^4He$ reactions for the experiment. The target, which has a height 1.8 m from the floor, is located at the center of a 5-m-square, 4.5-m-high target room. The room is surrounded by an ordinary concrete wall that is 1.5 to 2.5 m thick. The ceiling and the floor are also made of ordinary concrete that is 1.5 and 0.3 m thick, respectively. The surface of the concrete is covered with a 20-mm-thick mortar layer.

On the rotating target, 30 to 37 TBq (800 to 1000 Ci) of tritium was adsorbed in a titanium layer that was 2.5 mg/cm^2 thick and that was vacuum-deposited on an 0.8-mm-thick copper alloy (Amzirc) disk that was 230 mm in diameter. The target disk rotated at ~800 rpm. The deuteron beam was accelerated by 330 keV with an intensity of 20 mA at the target by the FNS accelerator system. This could provide a 4π neutron yield of 5×10^{12} n/s at the initial condition of the tritiated target. Considering the reaction kinematics and the deuteron energy loss in the tritium-titanium layer,[6] we used a Monte Carlo code to calculate the energy and angular dependence of the generated neutrons. From comparisons with the measurement, the accuracy of the calculated neutron spectrum was confirmed to be within 3%.

The absolute number of total neutrons generated from the target during the experiment was determined by counting the alpha particles from the $^3T(d,n)^4He$ reaction.[7] The associated alpha-particle detector with

a surface barrier semiconductor (SSD) was set in the beam drift chamber at an angle of 178.4 deg and at a distance 966.6 mm from the target. During the heavy irradiation above the 1-mA operation, external neutron monitors were used and calibrated by correspondence with the alpha-particle count at low intensity to avoid a pulse piling-up of the SSD system and self-radiation damage. For the external monitors, ^{238}U and ^{232}Th fission counters were used. The ^{238}U counter was located inside the experimental assembly, and the ^{232}Th counter was attached on the ceiling wall just above the target location.

The systematic errors of the absolute neutron yield Y_n in the alpha-particle counting method included uncertainties of the anisotropy correction factor and the solid angle $\Delta\Omega$ subtended by the SSD aperture. The uncertainty of the anisotropy correction factor was $\sim 1.5\%$, which was mainly due to nonuniformity of the tritium distribution caused by depletion of tritium with deuteron beam bombardment. The uncertainty of $\Delta\Omega$ was estimated to be 0.85%. The overall error in the measured neutron yield was $\sim 2\%$.

II.B. Experimental Assembly

The neutron source was surrounded by materials containing lithium to adjust the energy spectrum of neutrons striking the test blanket assembly as in a fusion reactor environment. Lithium carbonate (Li_2CO_3) was one such enclosure. This configuration was determined by precalculation for the experimental system selection.[8] Figure 1 shows the basic geometry of this experimental system. A detailed explanation of the foregoing dimensions and the material densities of the experimental system is given in Ref. 3. The test region made only of Li_2O, called the reference blanket, was replaced by the current heterogeneous test blankets. The cross section of the cavity was 862 mm square. The length of the cavity and the thickness of the test blanket region ranged from 1200 to 1242 mm and from 610 to 636 mm, respectively, according to the test configurations. The neutron source was positioned 458 mm from the back wall of the cavity.

The Li_2CO_3 was made into block form individually machined to dimensions of $51 \times 101.5 \times 203$ mm^3. The Li_2CO_3 surface was coated by an epoxy surface sealer to serve principally as a tritium barrier as well as to prevent moisture absorption. On the basis of an estimated 50-μm recoil range of triton, the epoxy was applied at a thickness of ~ 0.1 mm. The blocks were piled up to make a 203-mm-thick enclosure, and the ceiling part of the cavity was bolted to the upper frame. The penetration around a beam drift tube was completely filled with blocks shaped by machining. The outside of

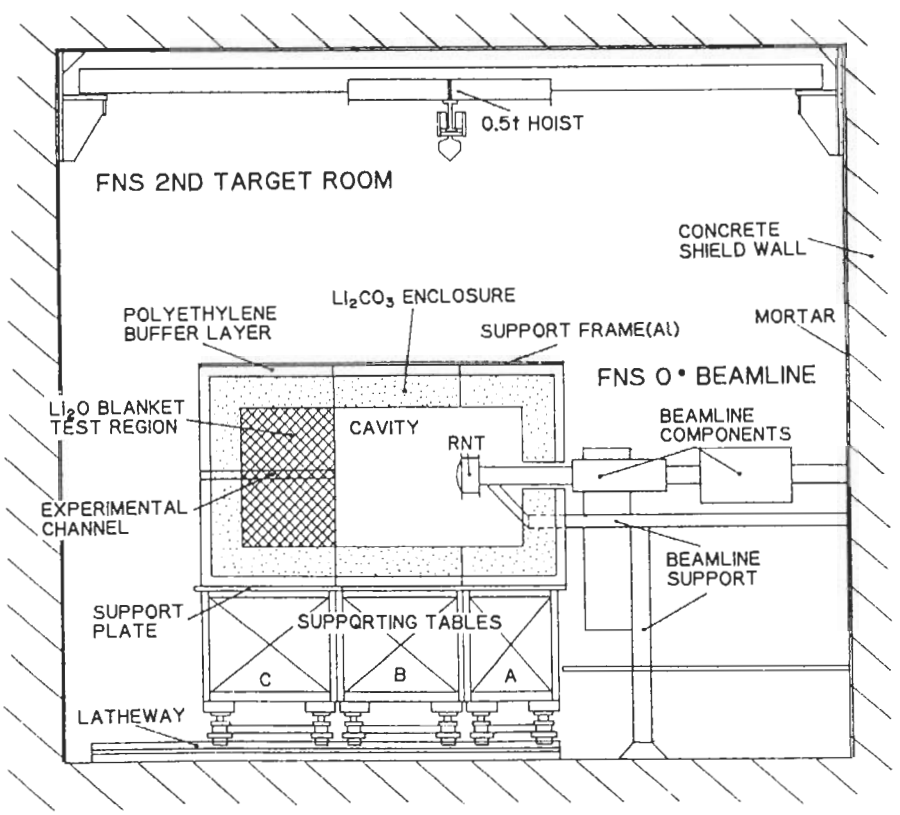

Fig. 1. Experimental arrangement of the closed geometry (Phase-II) by Li_2CO_3 enclosure.

the lithium enclosure was covered with 50-mm-thick polyethylene to protect the test blanket region from the room-returned neutrons.

II.C. BEO Test Blanket

The BEO arrangement was made of multiple layers of beryllium and Li_2O, as shown in Fig. 2 for the front and side views. The beryllium and the Li_2O layers were alternately piled up with blocks of each material. The edge-on structure was seen on the face of the test blanket, as shown in Fig. 3. The thicknesses of the beryllium and Li_2O layers were both 50.8 mm; consequently, the volume fraction was even. The beryllium was used as cubic blocks of $50.8 \times 50.8 \times 50.8$ mm^3 with a density of 1.837 g/cm^3. Three types of Li_2O were used for the tritium breeding material. The outside dimensions of these blocks were 50.6 mm square and 50.6, 101.2, or 202.4 mm in length. The bricks were made from Li_2O powder by cold pressing and covered with 0.2-mm-thick stainless steel. The impurity of the metal elements in the powder was <0.2%, except the lithium itself. The density of the Li_2O bricks was 75.5% of theoretical density, and the isotopic fraction of ^6Li was 7.41%. The impurities of H_2O and CO_2 in the bricks were kept <0.1%. The surface of the beryllium layer was located 779.7 mm from the source, and the surface of the Li_2O layer was just behind, so that the exact thicknesses of both layers in the mixed region were 304.8 and 300.3 mm, respectively. This mixed zone was followed by a 304-mm-thick Li_2O zone, and the overall size of the test blanket was 862 mm square with a Li_2O thickness of 604.3 mm.

The test blanket was equipped with four experimental drawers for the in-system measurements. The drawer system consisted of a sheath (a 0.2-mm-thick stainless steel guide sleeve) and a 0.2-mm-thick stainless steel drawer. For the on-line measurements, blocks with 22-mm-square holes were used to insert the signal cables. Two 125- and 428-mm-deep radial (the direction perpendicular to the beam axis) drawer channels and two axial (the direction parallel to the beam axis) drawer channels in the central and off-central axes (with a 100-mm interval) were installed.

II.D. Coolant Channel Test Blanket

Water coolant channels are usually designed with ~10-mm-diam stainless steel tubes in parallelepiped arrangement. This arrangement was simulated by two channels made of polyethylene and stainless steel plates in a face-on geometry, named the WCC test blanket,

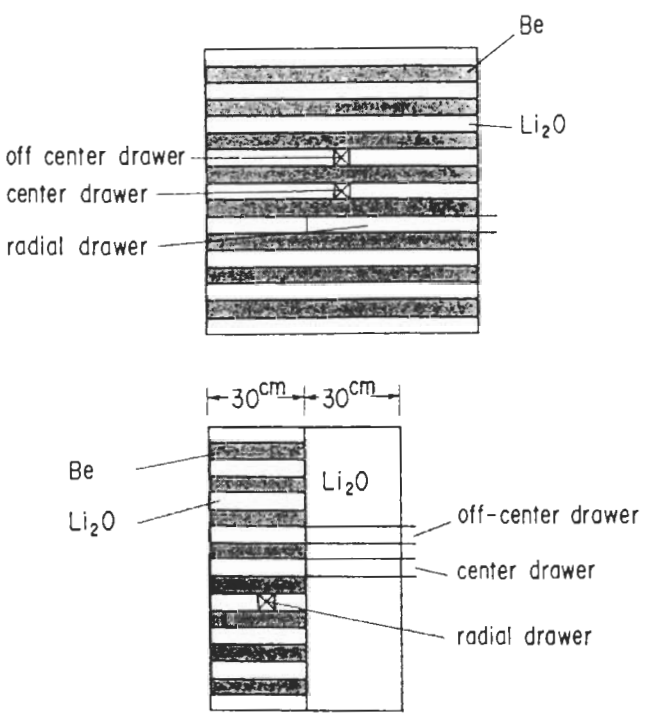

Fig. 2. The BEO test blanket configuration.

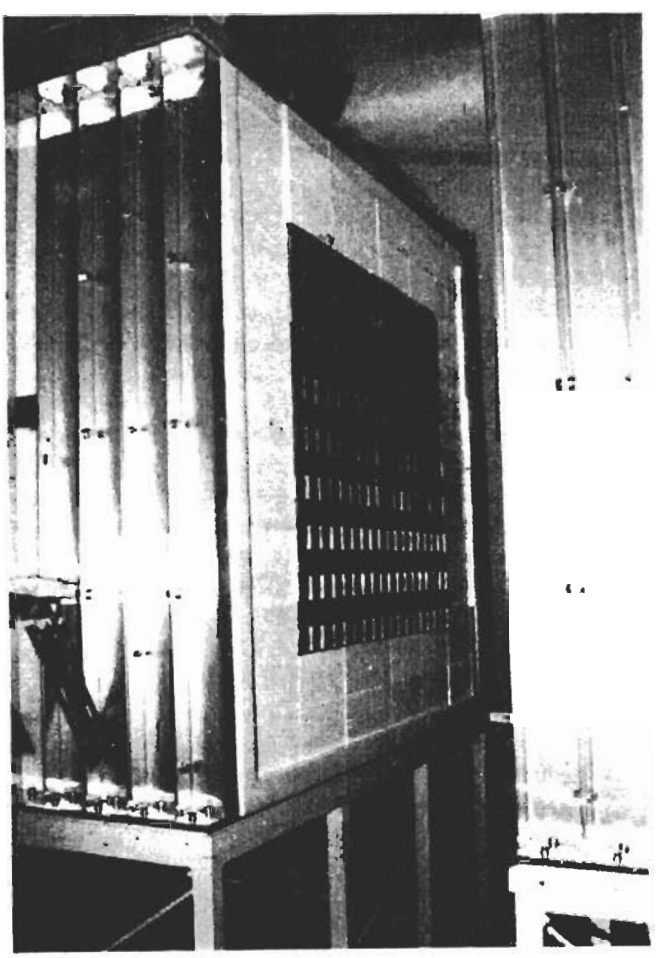

Fig. 3. Photograph of the front view of the BEO test blanket.

as shown in Fig. 4. This test blanket had the first wall with coolant structure and two coolant channels, and the rest was filled with Li_2O. The coolant channel zones were composed of a 5-mm-thick polyethylene plate sandwiched between 0.7-mm-thick Type 304 stainless steel plates. Each channel had a clearance of 0.6 to 1.1 mm because of the small curvature of the plate. The first wall was composed of a 5-mm-thick stainless steel plate. Polyethylene [the chemical form is assumed to be $(CH_2)_n$] was used for simulating water coolant, and its density was 0.9615 g/cm^3. The Li_2O blocks used here were the same that were used with the BEO blanket.

The first-wall surface was located 752.7 mm from the source, and the surface of the first Li_2O zone was 768.7 mm. The thicknesses of the three Li_2O zones were 100.5, 203, and 301.3 mm, respectively, and the overall thickness of the test blanket was 635.8 mm including the first wall. The radial experimental drawers were removed because of difficulty of setup.

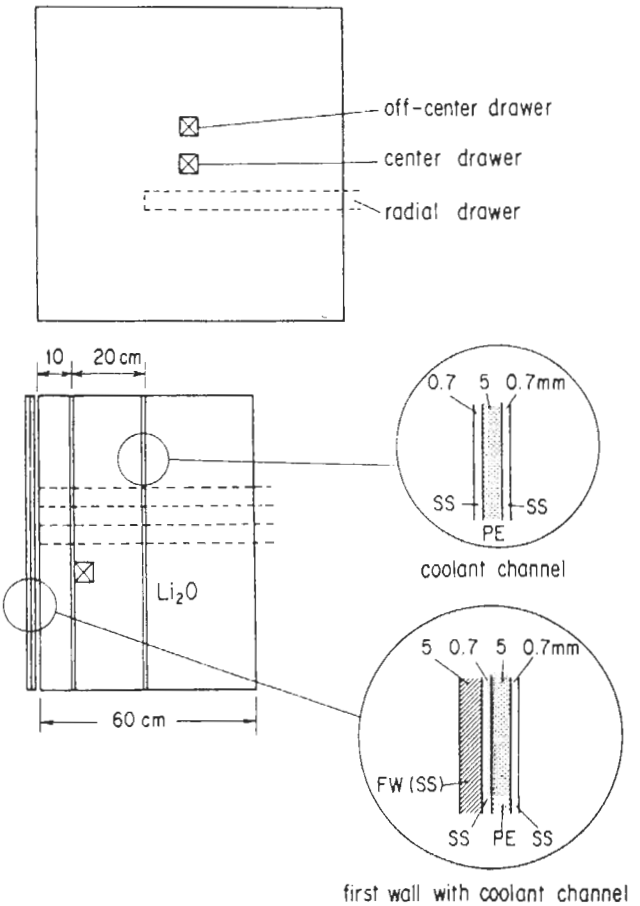

Fig. 4. The WCC test blanket configuration.

III. MEASUREMENT

Measurement techniques for nuclear parameters are most important in fusion blanket neutronics experiments. Several kinds of techniques were proposed and applied in previous collaborative work.[9] The following techniques were applied in the current experiments with a few modifications. The details of these techniques are reviewed elsewhere.[10]

III.A. Tritium Production

A metal foils scheme[11] was applied to direct measurement. Samples were encapsulated in pure aluminum to prevent tritiated gas from escaping. The sample size was 18 mm in diameter and 0.5 mm in thickness. The outer diameter including the aluminum capsule was 23.8 mm. Tritium was extracted from the samples by furnace digestion in a carrier hydrogen atmosphere and converted to HTO on a hot copper oxide surface. A liquid scintillation counting system was equipped for counting tritium decay. Calculations that yield the TPR of ^{6}Li and ^{7}Li per source neutron made use of foil pairs with different enrichment, exposed at the same location. The error for this method was estimated to be within 5% for the TPR including the neuton source yield error.

A zonal method[12] was also applied to tritium production measurement utilizing the breeding materials piled as a mass to act as the detectors themselves. This method uses a few different sizes of cold-pressed bricks ranging from 48 mm square and 12 to 48 mm in thickness employing a granule type of Li_2O powder. Heating under a vacuum was applied for tritium extraction from irradiated bricks as well as for the Li-metal foil scheme. The extracted tritium was converted to HTO by a CuO furnace, and 6 cm^3 of tritiated water was mixed with 14 cm^3 of scintillation liquid (Aquasol-2). The scintillation cocktail was counted by a liquid scintillation counting system. The overall experimental errors were expected to be 3% because of a better signal-to-background ratio.

An on-line method is very useful compared with the foregoing time-consuming method when a quick measurement is required for many measuring points and for comparative study among experimental systems. For this purpose, the TPR of ^{6}Li was measured by using the different responses between the ^{6}Li-glass and ^{7}Li-glass scintillators.[13] Because one can assume that the gamma-ray responses of both scintillators are almost identical if the irradiation field is identical, the gamma-ray background can be removed by subtracting the pulse-height spectrum of ^{7}Li-glass from that of ^{6}Li-glass. The glass scintillator of 10-mm diameter and 0.3-mm thickness was chosen to compromise the self-shielding and the wall escape effects. Systematic errors come mainly from those of the source neutron yield and the atomic number of ^{6}Li. The ^{6}Li atomic number was determined by isotope dilution analysis within an uncertainty of ~0.5%. The statistical error of the ^{6}Li$(n,\alpha)^3$T reaction counting was 0.3 to 1.1%. The

fitting error was also considered in the pulse-height subtraction where the Gaussian response was assumed.

An NE-213 scintillation spectrometer was also applied to obtain the TPR of ^7Li for on-line measurement. The threshold energy of the $^7Li(n,n'\alpha)^3T$ reaction was ~3 MeV, while the measuring energy range of the NE-213 was above 1 MeV. Then, the TPR from ^7Li was estimated from the neutron spectrum measured by the NE-213 spectrometer described later with the data of the $^7Li(n,n'\alpha)^3T$ reaction cross section. The cross section of ^7Li used in the current experiment was retrieved from the JENDL-3PR2 evaluated at JAERI (Ref. 14). Note that these TPR distributions are biased by the data of JENDL-3PR2. The overall error possibly becomes >5% when the cross-section error is included.

III.B. Neutron Spectrum

Two kinds of miniature neutron spectrometers were used for in situ measurement. One was an NE-213 scintillator for neutrons in the mega-electron-volt region, and the other was a proton-recoil gas proportional counter (PRC) in the kilo-electron-volt region.

A small spherical detector with an NE-213 liquid scintillator was developed to meet the requirements for in situ measurement.[15] This detector has good neutron response and pulse-shape discrimination characteristics for that purpose. An NE-213 liquid of 1.38×10^3 mm^3 was contained in a 14-mm-diam spherical cell made of 1-mm-thick Pyrex glass. Two pulse-height spectra with different gains were combined at ~2 MeV and unfolded by the FORIST code[16] by using the neutron response matrix previously determined by the Monte Carlo method. The overall error was 4% for the flux above 10 MeV and 10 to 20% below 10 MeV depending on the spectrum shape.

The PRC used here was originally developed and modified to small size for in situ measurement by Bennett at Argonne National Laboratory.[17] The counter body is fabricated from 0.41-mm-thick Type 304 stainless steel alloy. The inner diameter and the effective length are 18.2 and 127 mm, respectively. To encompass the neutron spectrum over the energy range from a few kilo-electron-volts to 1 MeV, we used two different gas fillings for identical counters: hydrogen at 5.5 atm with 1% CH_4 for the low-energy component and a 50-50 mixture of hydrogen and argon at 8.8-atm for the upper energy component. Argon increases the stopping power, thereby reducing the proton-recoil range. Four high-voltage runs were performed to measure the neutron spectra at the energy region from a few kilo-electron-volts to 150 keV. Three high-voltage runs for the hydrogen/argon counter were done at the energy region from 150 keV to 1 MeV. The neutron spectrum was derived from the recoil proton spectrum by using the derivative method. The overall error was expected to be ~10%.

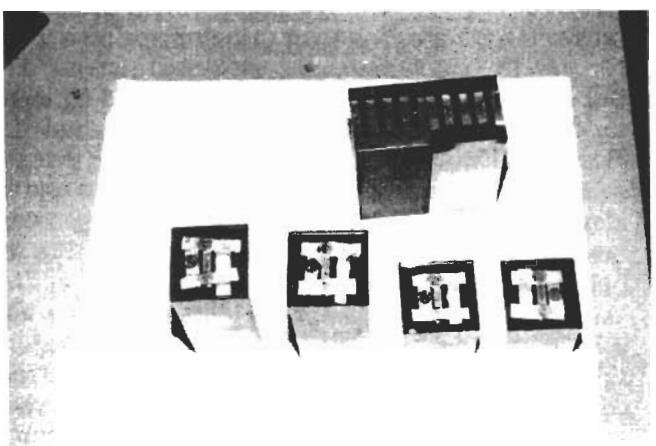

Fig. 5. Foil setup for activation measurement between the stacked blocks.

III.C. Reaction Rate

The foil activation technique was employed to give the in-system neutron spectrum indices. The dosimetry reactions used were $^{27}Al(n,\alpha)^{24}Na$, $^{56}Fe(n,p)^{56}Mn$, $^{58}Ni(n,p)^{58}Co$, $^{58}Ni(n,2n)^{57}Ni$, $^{90}Zr(n,2n)^{89}Zr$, $^{93}Nb(n,2n)^{92m}Nb$, $^{115}In(n,n')^{115m}In$, $^{197}Au(n,\gamma)^{198}Au$, and so on. The sizes of the foils were 10 mm in diameter and 1 mm in thickness, and the size for gold was $5 \times 10 \times 0.001$ mm. The cross sections of these reactions[18] were also measured at ~14 MeV. The foils were emplaced between the stacked Li_2O blocks, as shown in Fig. 5, and irradiated for ~10 h with D-T neutrons. Total neutron yields at the target were 4.3×10^{16} neutrons in the BEO experiment and 7.4×10^{16} neutrons in the WCC experiment, respectively. The neutron intensity variation during irradiation was recorded by using multichannel scaling to make the decay correction at the time of gamma-ray measurement. Gamma rays were measured with germanium detectors, and the reaction rates were reduced with the decay time, branching ratio, and so on. The self-shielding effect for the gold foil was negligible for most of the measurements with Li_2O because of a low flux of low-energy neutrons and the usage of very thin foil of 0.01 mm. However, a flux depression of ~5% was still estimated for the 5-eV resonance of the $Au(n,\gamma)$ reaction at the inside of the beryllium where many low-energy neutrons exist. The overall error for the major part of the reaction rate ranged from 3 to 6%.

IV. RESULTS AND DISCUSSION

IV.A. Experimental Results

A long irradiation run followed by passive detector measurements was performed by deuteron beam irradiation of ~20 mA and 10 h for the zonal block,

Li-metal, and foil activation methods measurements, while on-line measurements were run at each position by beams of 10 μA to 1 mA and for a few minutes for the Li-glass and the NE-213 scintillators and the gas proportional counter. All of the measured data were normalized to the values corresponding to one source neutron emission at the target.

IV.A.1. BEO Blanket

The obtained TPR results are shown in Fig. 6 and summarized in Table I for the on-line counter methods. The results were normalized to the reaction probability per one lithium atom when one neutron was produced at the neutron target. The distances denote the position of the detector center from the target. The TPRs in the Li_2O zones were measured by means of the zonal block method with 5-cm Li_2O cubic samples emplaced in the central and off-central drawer channels. The off-central drawer was filled with lithium blocks of natural content while the central drawer was partly filled with ^{7}Li enriched blocks. The results listed in Table II are the averaged TPRs over the volume of 5 cm cubic for natural lithium in the off-center axis and ^{7}Li enriched lithium in the central axis. On the other hand, the Li-glass method obtained the TPR averaged over the detector volume of 10 mm in diameter and 0.3 mm in thickness. The on-line detector may bring the void due to detector body and cables. These averaging and void effects are discussed in Sec. IV.B.

The reflected neutron component from the cavity on the surface of the BEO blanket was estimated by using the NE-213 spectrometer, as shown in Fig. 7. The measurement was performed with and without the test blanket to separate its contribution. One can clearly see that the reflection from the test blanket contributed only to the flux below 10 MeV and by ~30% of the total reflected components on its surface. Figure 8 shows the results of the in situ neutron spectrum measurement in the Li_2O layer. The PRC covered the energy range of 3 keV to 1 MeV, and the NE-213 detector covered the energy range from 2 to 15 MeV. We set the axis of

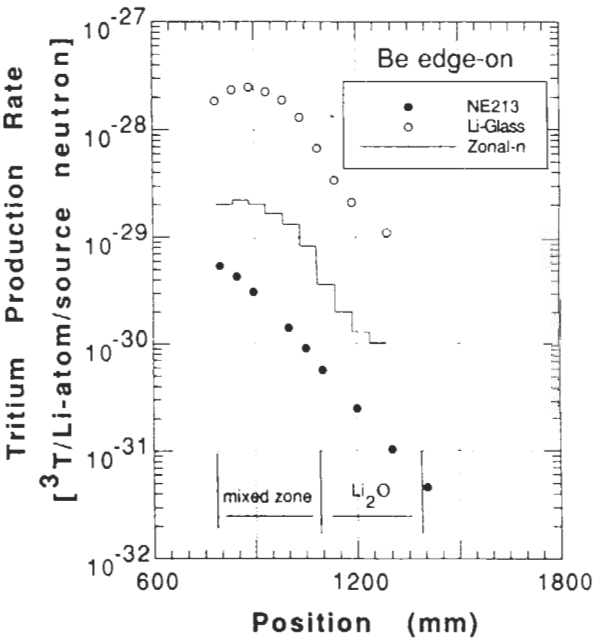

Fig. 6. Measured TPRs with three different methods in the BEO blanket.

TABLE I

TPRs Measured by NE-213 and Li-Glass Scintillators Along the Central Axis in the BEO Experiment

Distance from Target (mm)	TPR[a] from ^{7}Li by NE-213	Distance from Target (mm)	TPR from ^{6}Li by Li-Glass
734.2	(5.77 ± 0.63)E−30[b]	784.1	(1.85 ± 0.08)E−28
796.2	(5.48 ± 0.49)E−30	833.5	(2.36 ± 0.10)E−28
846.2	(4.34 ± 0.34)E−30	884.1	(2.49 ± 0.09)E−28
897.2	(3.13 ± 0.23)E−30	934.7	(2.27 ± 0.08)E−28
999.2	(1.43 ± 0.10)E−30	985.3	(1.89 ± 0.07)E−28
1051.2	(9.17 ± 0.62)E−31	1035.9	(1.31 ± 0.05)E−28
1100.2	(5.75 ± 0.39)E−31	1086.5	(6.78 ± 0.26)E−29
1201.2	(2.51 ± 0.17)E−31	1137.1	(3.40 ± 0.16)E−29
1302.2	(1.04 ± 0.07)E−31	1187.7	(2.14 ± 0.09)E−29
1404.2	(4.66 ± 0.33)E−32	1288.9	(1.12 ± 0.05)E−29
1505.2	(1.91 ± 0.18)E−32	1391.3	(8.66 ± 0.33)E−30
		1492.9	(6.87 ± 0.27)E−30

[a]Units are in tritium atoms per lithium atom per source neutron.
[b]Read as (5.77 ± 0.63) × 10^{-30}.

TABLE II

TPRs of Li_2O Zones Measured by Zonal Technique Along the Central Axis in the BEO Experiment

Distance of Zone Boundary from Target (mm)	TPR[a] from ^{6}Li by Zonal Method	TPR from ^{7}Li by Zonal Method
784.2 to 835.2	(2.04 ± 0.06)E−29[b]	(5.51 ± 0.17)E−30
835.2 to 883.2	(2.21 ± 0.07)E−29	---
883.6 to 933.2	(2.03 ± 0.06)E−29	(3.23 ± 0.10)E−30
933.2 to 984.2	(1.67 ± 0.05)E−29	---
984.2 to 1033.8	(1.33 ± 0.04)E−29	(1.47 ± 0.04)E−30
1033.8 to 1081.8	(8.31 ± 0.25)E−30	---
1086.2 to 1136.4	(3.67 ± 0.11)E−30	(5.56 ± 0.17)E−31
1136.4 to 1187.4	(2.01 ± 0.06)E−30	---
1187.4 to 1238.4	(1.30 ± 0.04)E−30	---
1238.4 to 1286.4	(1.03 ± 0.03)E−30	(1.99 ± 0.06)E−31

[a]Units are in tritium atoms per lithium atom per source neutron.
[b]Read as (2.04 ± 0.06) × 10^{-29}.

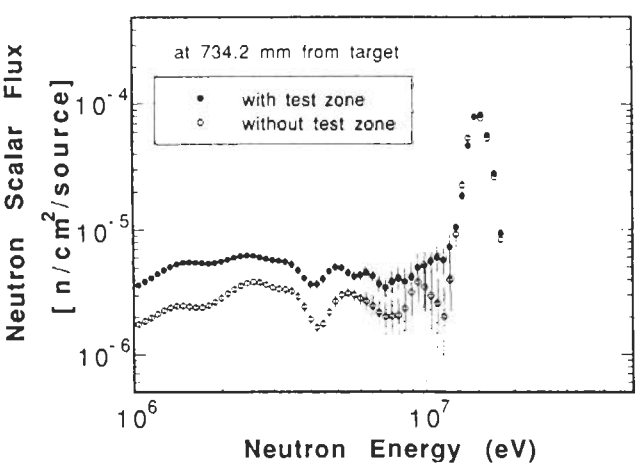

Fig. 7. Neutron spectra measured at the surface position of the BEO test blanket with and without the blanket. The difference indicates the reflection neutron component from the test blanket.

the PRC in the radial direction using a radial drawer, assuming horizontal uniformity, while we set the spherical NE-213 detector in the central drawer. The gross spectrum shape did not change much except for the height of the 14.8-MeV peak and except for being below 200 keV. The peak of the incident energy decreased rapidly more than one order after 300 mm of depth, but the low-energy flux below the Li(n,α) resonance reaction of 250 keV decreased only one-fifth. The unreasonable decrease of the flux below 10 keV may have been caused by a change in the ionization energy of the gas in the multiplication process.

Several reaction rate distributions along the central

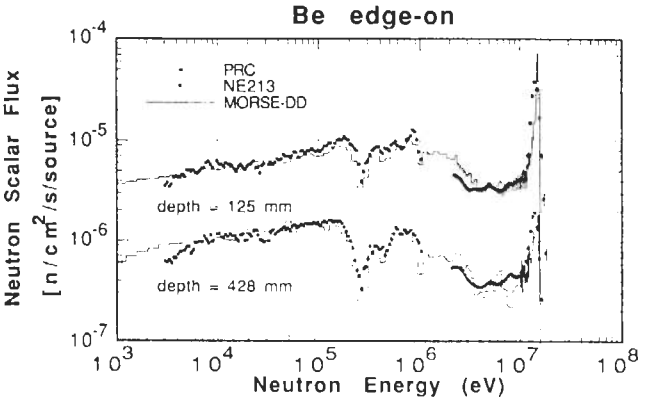

Fig. 8. In-system neutron spectra at two different positions in the BEO blanket measured by the NE-213 scintillator and the PRC. The step line shows the calculated spectra obtained by MORSE-DD.

axis are summarized in Table III for the ^{93}Nb$(n,2n)$, ^{27}Al(n,α), ^{58}Ni(n,p), ^{58}Ni$(n,2n)$, ^{115}In(n,n'), and ^{197}Au(n,γ) reactions and are shown in Fig. 9. One can see that the lower threshold reaction distributions, e.g., ^{27}Al(n,α) and ^{58}Ni(n,p), were similar to those of the ^{7}Li TPR, while the reaction distribution of the ^{197}Au(n,γ) reaction was very similar to the ^{6}Li TPR distribution. The difference between the high-threshold and the lower threshold reactions was in the slopes of the axial distributions at the front region of the test blanket. In the front, slowing-down neutrons continued to

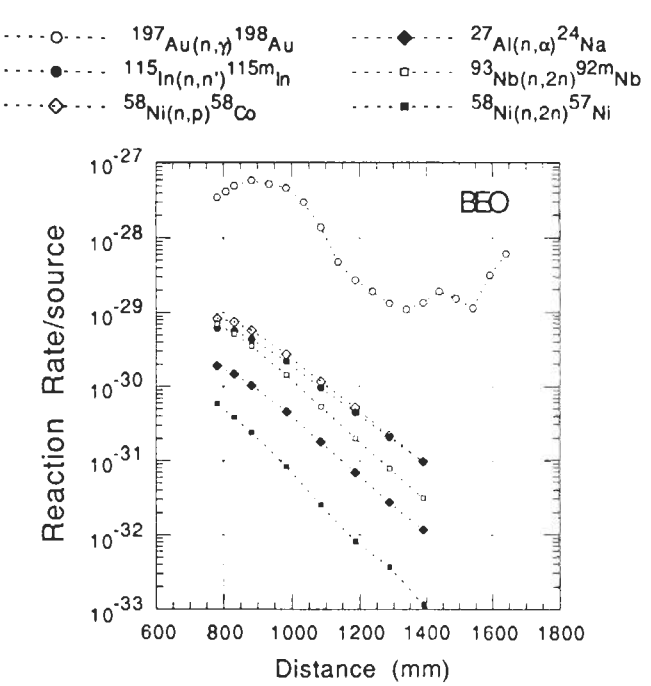

Fig. 9. Measured reaction rate distributions for activation reactions in the BEO blanket.

TABLE

Activation Reaction Rates Measured Along

Distance from Target (mm)	$^{197}Au(n,\gamma)^{198}Au$	$^{115}In(n,n')^{115m}In$	$^{58}Ni(n,p)^{58}Co$
781.2	(3.44 ± 0.11)E−28[a]	(6.07 ± 0.17)E−30	(8.27 ± 0.25)E−30
806.3	(4.13 ± 0.13)E−28	---	---
831.8	(4.93 ± 0.15)E−28	(5.61 ± 0.17)E−30	(7.37 ± 0.22)E−30
882.7	(5.76 ± 0.19)E−28	(4.32 ± 0.13)E−30	(5.66 ± 0.17)E−30
933.7	(5.16 ± 0.17)E−28	---	---
984.2	(4.59 ± 0.15)E−28	(2.19 ± 0.07)E−30	(2.73 ± 0.08)E−30
1036.0	(2.94 ± 0.10)E−28	---	---
1085.7	(1.37 ± 0.05)E−28	(9.59 ± 0.29)E−31	(1.17 ± 0.04)E−30
1136.4	(4.66 ± 0.16)E−29	---	---
1187.4	(2.66 ± 0.08)E−29	(4.49 ± 0.14)E−31	(5.20 ± 0.16)E−31
1238.2	(1.88 ± 0.06)E−29	---	---
1288.7	(1.31 ± 0.04)E−29	(2.06 ± 0.07)E−31	(2.18 ± 0.07)E−31
1339.7	(1.10 ± 0.04)E−29	---	---
1390.2	(1.34 ± 0.04)E−29	(9.56 ± 0.33)E−32	(9.67 ± 0.31)E−32
1439.2	(1.88 ± 0.06)E−29	---	---
1490.2	(1.52 ± 0.05)E−29	---	---
1541.2	(1.14 ± 0.04)E−29	---	---
1591.9	(3.09 ± 0.09)E−29	---	---
1641.2	(5.99 ± 0.18)E−29	---	---

[a]Units are in reactions per atom per source neutron. Read as $(3.44 \pm 0.11) \times 10^{-28}$.

stay above the threshold for the low-threshold group, and they decreased after passing a certain depth. On the other hand, the high-threshold reactions decreased from the front region. Reaction rates of nonthreshold reactions such as $^{197}Au(n,\gamma)$ were also enhanced by the upper and lower beryllium as well as the $^{6}Li(n,\alpha)$ reaction. A vertical distribution of the $^{197}Au(n,\gamma)$ reaction was measured across the beryllium and the Li_2O layers from the bottom to the top by stacking small and thin foils between the blocks. An oscillation effect, a large peak in the beryllium zone and a deep valley in the Li_2O zone, was seen in the distributions measured at the surface and at a 100-mm depth in the Be/Li_2O mixed zone, as shown in Fig. 10. The peak in beryllium was attributable to the enhanced low-energy neutron flux due to slowing down by beryllium, and a large absorption of low-energy neutrons in the Li_2O region through the $^{6}Li(n,\alpha)T$ reaction gave a lower reaction rate for $^{197}Au(n,\gamma)^{198}Au$. The distribution at 100-mm depth showed large oscillation and lower values at both edges of the test blanket, but the distribution was periodically symmetric in the central region within a 500-mm width.

IV.A.2. WCC Blanket

In this experiment, the Li-metal foil technique was applied for the TPR measurements in addition to the techniques used in the BeO experiment. The pairs of Li-foils of enriched ^{7}Li (0.003% ^{6}Li) and natural lithium (7.578% ^{6}Li) were irradiated between the Li_2O blocks in the drawer. The ^{6}Li results were reduced by the ^{n}Li

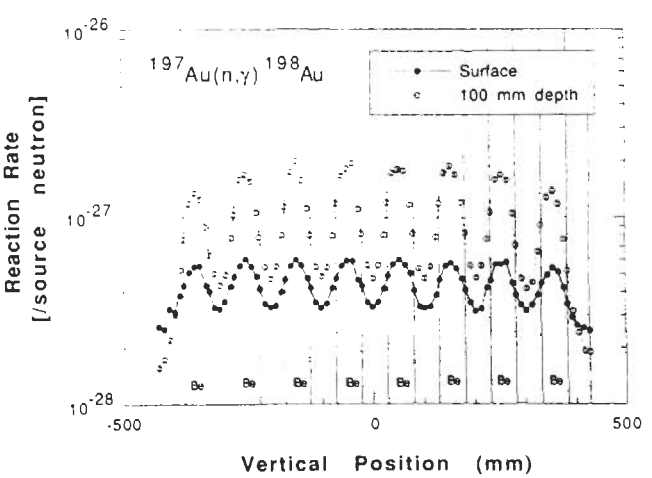

Fig. 10. Reaction rate distribution of the $^{197}Au(n,\gamma)^{198}Au$ reaction measured across the piled-up layers of the beryllium and the Li_2O at the surface and at a 100-mm depth from the surface in the BEO blanket.

III

the Central Axis in the BEO Experiment

$^{27}Al(n,\alpha)^{24}Na$	$^{93}Nb(n,2n)^{93m}Nb$	$^{58}Ni(n,2n)^{57}Ni$
(1.90 ± 0.06)E−30	(6.94 ± 0.19)E−30	(5.82 ± 0.17)E−31
---	---	---
(1.47 ± 0.04)E−30	(5.08 ± 0.15)E−30	(3.77 ± 0.12)E−31
(1.04 ± 0.03)E−30	(3.49 ± 0.10)E−30	(2.38 ± 0.08)E−31
---	---	---
(4.56 ± 0.14)E−31	(1.43 ± 0.04)E−30	(8.28 ± 0.28)E−32
---	---	---
(1.77 ± 0.05)E−31	(5.30 ± 0.16)E−31	(2.53 ± 0.09)E−32
---	---	---
(6.93 ± 0.21)E−32	(2.00 ± 0.06)E−31	(8.16 ± 0.45)E−33
---	---	---
(2.73 ± 0.10)E−32	(7.82 ± 0.23)E−32	(3.65 ± 0.39)E−33
---	---	---
(1.16 ± 0.04)E−32	(3.12 ± 0.10)E−32	(1.16 ± 0.15)E−33
---	---	---
---	---	---
---	---	---
---	---	---
---	---	---

and the ^{7}Li TPRs by using the isotropic ratio because a significant self-shielding effect was expected for ^{6}Li-metal. Because the void effect, i.e., the effect of losing the channel as a result of placement of the measurement hole, was expected to be large for the TPR response of ^{6}Li, the on-line measurement was performed only at the back of each coolant channel. On the other hand, there was no void for the Li-metal and zonal measurements because of their direct stacking between the blocks. The results for the TPRs are summarized in Table IV and shown in Fig. 11. The ^{7}Li TPR distribution was shifted down by ~25% from the previous BEO because of the existence of the first wall. The ^{6}Li TPR was quite differently shaped and showed a factor of 2 larger enhancement around the WCCs.

In situ spectrum measurement was performed only by the small sphere NE-213 spectrometer in this experiment because there was no good space in the test blanket to locate the PRC, which required a radial drawer. The spectrum obtained from the NE-213 spectrometer was lower at the peak than was the previous arrangement.

The reaction rate distributions along the central axis of the $^{197}Au(n,\gamma)$, $^{115}In(n,n')$, $^{58}Ni(n,p)$, $(n,2n)$, $^{27}Al(n,\alpha)$, and $^{93}Nb(n,2n)$ reactions were measured as well as the BEO arrangement, and the results are summarized in Table V, as shown in Fig. 12. A fine

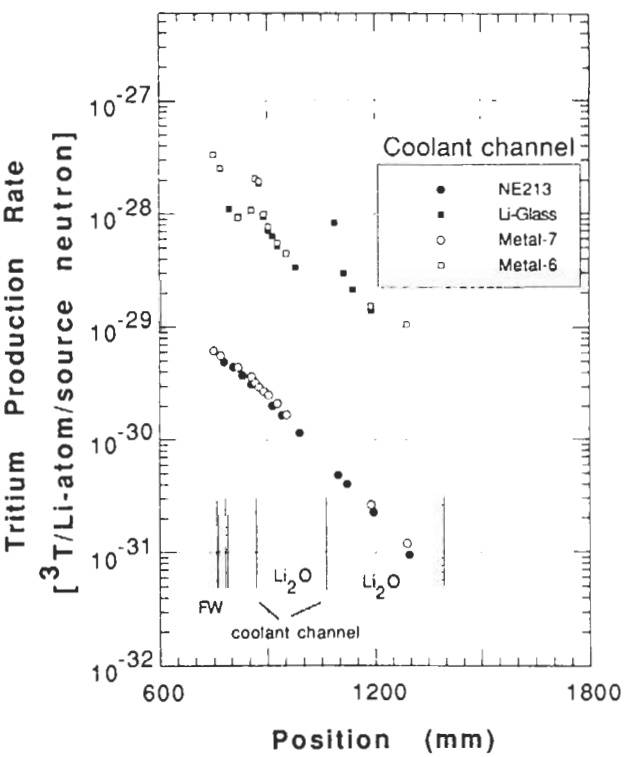

Fig. 11. Measured TPRs with three different methods in the WCC blanket.

TABLE IV

TPRs Measured by NE-213, Li-Glass Scintillators and Li-Metal Foil Along the Central Axis in the WCC Experiment

Distance from Target (mm)	TPR[a] from ^{7}Li by NE-213	Distance from Target (mm)	TPR from ^{6}Li by Li-Glass	Distance from Target (mm)	TPR from ^{7}Li by Li-Metal	TPR from ^{6}Li by Li-Metal
780.7	(4.93 ± 0.50)E−30[b]	795.2	(1.11 ± 0.04)E−28	745.0	(6.24 ± 0.31)E−30	(3.34 ± 0.17)E−28
805.7	(4.44 ± 0.40)E−30	820.5	(9.29 ± 1.10)E−29	762.0	(5.64 ± 0.28)E−30	(2.52 ± 0.13)E−28
830.7	(3.76 ± 0.31)E−30	877.4	(1.87 ± 0.08)E−28	812.0	(4.39 ± 0.22)E−30	(9.26 ± 0.46)E−29
855.7	(3.14 ± 0.26)E−30	890.0	(9.53 ± 0.36)E−29	849.0	(3.64 ± 0.18)E−30	(1.08 ± 0.05)E−28
915.2	(2.02 ± 0.16)E−30	902.7	(7.14 ± 0.31)E−29	861.0	(3.26 ± 0.16)E−30	(2.06 ± 0.10)E−28
940.2	(1.67 ± 0.13)E−30	915.3	(6.40 ± 0.56)E−29	870.0	(2.96 ± 0.15)E−30	(1.96 ± 0.10)E−28
990.2	(1.16 ± 0.09)E−30	928.0	(5.18 ± 0.43)E−29	889.0	(2.72 ± 0.14)E−30	(9.94 ± 0.50)E−29
1096.7	(4.85 ± 0.38)E−31	953.3	(4.48 ± 0.22)E−29	896.0	(2.52 ± 0.14)E−30	(7.68 ± 0.38)E−29
1121.7	(4.05 ± 0.32)E−31	978.6	(3.37 ± 0.21)E−29	921.0	(2.12 ± 0.11)E−30	(5.55 ± 0.28)E−29
1196.7	(2.25 ± 0.18)E−31	1088.1	(8.29 ± 0.26)E−29	946.0	(1.68 ± 0.08)E−30	(4.47 ± 0.22)E−29
1297.7	(9.51 ± 0.89)E−31	1113.5	(2.98 ± 0.13)E−29	1161.0	(2.63 ± 0.13)E−31	(1.53 ± 0.08)E−29
		1138.8	(2.13 ± 0.09)E−29	1262.0	(1.20 ± 0.06)E−31	(1.06 ± 0.05)E−29
		1189.4	(1.41 ± 0.08)E−29			

[a]Units are in tritium atoms per lithium atom per source neutron.
[b]Read as $(4.93 \pm 0.50) \times 10^{-30}$.

TABLE

Activation Reaction Rates Measured Along

Distance from Target (mm)	$^{197}Au(n,\gamma)^{198}Au$	$^{115}In(n,n')^{115m}In$	$^{58}Ni(n,p)^{58}Co$
752.7	(5.70 ± 0.17)E−28[a]	---	(7.87 ± 0.24)E−30
769.9	(7.28 ± 0.23)E−28	(5.67 ± 0.17)E−30	(7.67 ± 0.24)E−30
820.8	(1.52 ± 0.05)E−28	---	---
869.1	(4.18 ± 0.13)E−28	---	---
875.3	(4.53 ± 0.14)E−28	---	---
877.8	(4.03 ± 0.12)E−28	(3.42 ± 0.11)E−30	(4.50 ± 0.14)E−30
979.1	(4.07 ± 0.13)E−29	(1.88 ± 0.06)E−30	(2.30 ± 0.07)E−30
1077.7	(1.89 ± 0.06)E−28	---	---
1084.5	(1.84 ± 0.06)E−28	---	---
1087.0	(1.76 ± 0.06)E−28	(8.47 ± 0.26)E−31	(1.02 ± 0.04)E−30
1188.4	(1.59 ± 0.05)E−29	(4.33 ± 0.14)E−31	(4.83 ± 0.16)E−31
1289.6	(9.09 ± 0.35)E−30	(2.02 ± 0.07)E−31	(2.19 ± 0.09)E−31
1337.9	(7.87 ± 0.27)E−30	---	---
1386.0	(1.01 ± 0.04)E−29	(1.02 ± 0.04)E−31	(9.85 ± 0.07)E−32
1439.5	(1.47 ± 0.06)E−29	---	---
1490.4	(1.33 ± 0.05)E−29	---	---
1541.4	(1.20 ± 0.05)E−29	---	---
1592.3	(2.75 ± 0.10)E−29	---	---
1616.7	(5.91 ± 0.22)E−29	---	---

[a]Units are in reactions per atom per source neutron. Read as $(5.70 \pm 0.17) \times 10^{-28}$.

distribution of the $^{197}Au(n,\gamma)$ reaction rate was obtained around the coolant channel by setting the foils between two triangle blocks forming a cubic. This scheme can provide the data with a 6-mm interval, as shown in Fig. 13. As expected, a steep increase in the $^{197}Au(n,\gamma)^{198}Au$ reaction rates was observed at a distance <35 mm from the boundary of the simulated coolant channels. This was due to the increase of the thermal neutrons in the coolant zone by the neutron scattering reactions with hydrogen.

IV.B. Detector Void Effect

The obtained vertical distribution of the $^{197}Au(n,\gamma)$ reaction showed a steep change when crossing the material boundary, e.g., between beryllium or hydrogen and Li_2O. The distribution of the ^6Li TPR was also expected to vary in such a boundary because of a large absorption cross section by ^6Li for low-energy neutrons. This easily reminds us of the void effect in the measurement of the Li-glass detector, which uses the measurement hole to insert the photomultiplier tube where no absorption material exists. This void would increase the neutron flux around the detector due to no absorption so that the measured response could overestimate the ^6Li TPR. To estimate this effect, we

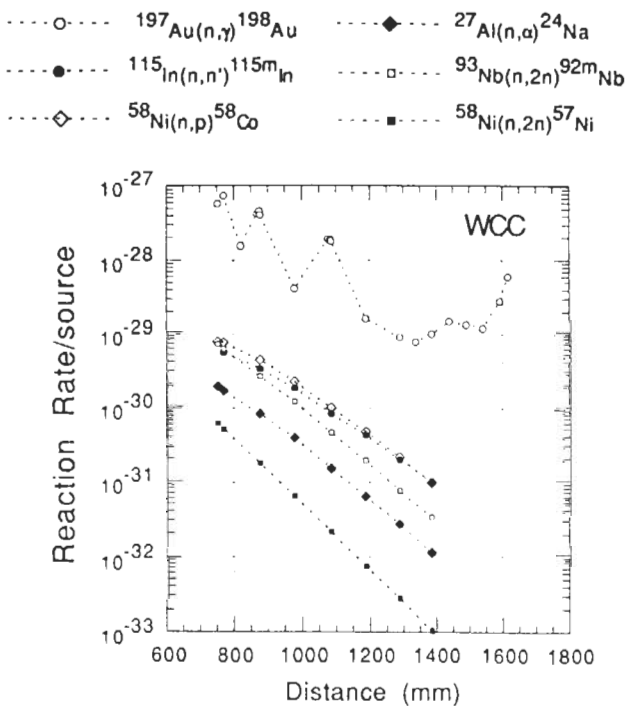

Fig. 12. Measured reaction rate distributions for activation reactions in the WCC blanket.

V

the Central Axis in the WCC Experiment

$^{27}Al(n,\alpha)^{24}Na$	$^{93}Nb(n,2n)^{93m}Nb$	$^{58}Ni(n,2n)^{57}Ni$
(1.97 ± 0.06)E−30	(7.24 ± 0.21)E−30	(6.21 ± 0.21)E−31
(1.72 ± 0.05)E−30	(6.26 ± 0.19)E−30	(5.19 ± 0.17)E−31
---	---	---
---	---	---
---	---	---
(8.41 ± 0.27)E−31	(2.70 ± 0.09)E−30	(1.79 ± 0.06)E−31
(3.95 ± 0.13)E−31	(1.22 ± 0.04)E−30	(6.54 ± 0.25)E−32
---	---	---
---	---	---
(1.52 ± 0.05)E−31	(4.67 ± 0.14)E−31	(2.16 ± 0.09)E−32
(6.41 ± 0.22)E−32	(1.95 ± 0.06)E−31	(7.44 ± 0.41)E−33
(2.72 ± 0.10)E−32	(7.69 ± 0.25)E−32	(2.78 ± 0.30)E−33
---	---	---
(1.15 ± 0.05)E−32	(3.37 ± 0.11)E−32	(1.05 ± 0.14)E−33
---	---	---
---	---	---
---	---	---
---	---	---
---	---	---
---	---	---

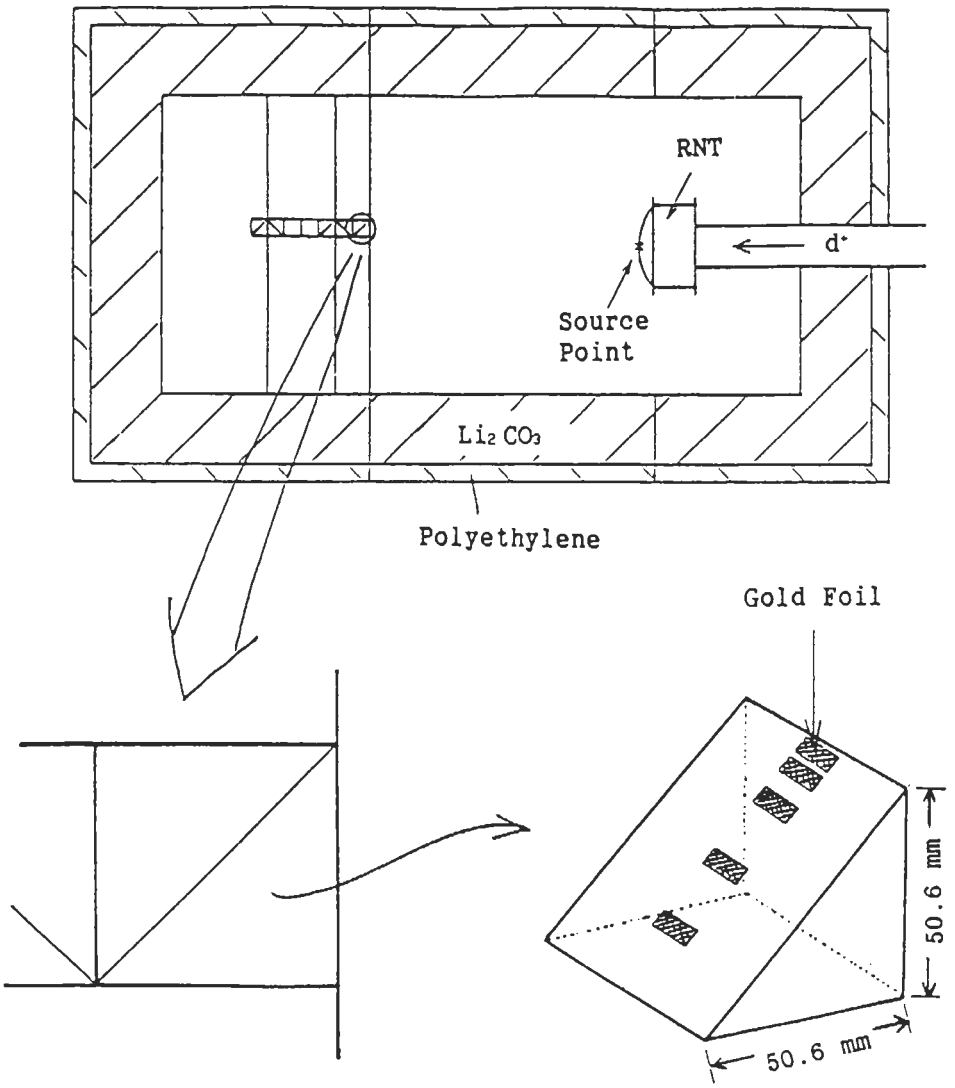

Fig. 13. Illustration of activation foil stacking method for detailed distribution measurement around the coolant channel.

measured the TPR distributions of the Li_2O layer in the vertical direction, where the beryllium and the Li_2O layers were piled up, with the zonal method using thin Li_2O plates. The measured distribution of the ^6Li TPR in a vertical direction inside the drawer was calculated from the results of natural and ^7Li zonal plate measurements, and each measurement represented the TPR averaged over the volume of a 9.6-mm-thick plate placed horizontally. One equivalent cubic block was made of five plates, and the average of those TPRs was ~20% higher than that of the central plate.

This distortion of the TPR due to the void was also estimated by calculation with the DOT3.5 two-dimensional neutron transport code.[19] The calculation model assumed annular symmetry of each layer and adopted cylindrical geometry (r-z), taking the central axis for the z axis. Hence, the beryllium and the Li_2O layers were modeled to cylinders. In the calculation, a 20-mm-diam and 20-mm-thick void was placed at a depth 125 mm from the blanket surface on the z axis in the calculation. As Table VI indicates, the void effect on the measurement by the Li-glass method with a 10-mm diameter was estimated to be 17% while the ratio of the Li-glass data to the center plate value of the zonal method was 20%. These numbers are very close. Figure 14 schematically shows the relation of the TPR distributions for both with and without the void, and the zonal measurement. One can see that the value obtained by the Li-glass detector is close to the value of the average, but it overestimates the point data at the center.

Another void effect existed in the measurement of the ^7Li TPR by the NE-213 detector: The front space of the scintillator probe replaced the Li_2O, and the

TABLE VI

Void Effect Estimation Due to the Detector on the ^6Li TPR with Calculation and Measurement at the 883.6- to 933.2-mm Zone

Calculation	Void/No Void	Measurement	
Effect on the region averaged over a 10-mm-diam zone for a 20-mm-diam void	1.17	Ratio of Li-glass value[a] to the center plate of the zonal result	1.20
Effect on the region averaged over a 20-mm-diam void	1.15	Ratio of the average of[b] zonal results to the value of the center plate	1.18

[a]Corresponding to the overestimation by the Li-glass method to the point data.
[b]Corresponding to the overestimation by the zonal method to the point data.

penetration length of the neutron to the detected point was different from that inside the complete assembly without the experimental hole. So, the obtained results may have been higher than the true ones especially at the front region where the uncollided neutron component was large. This effect was estimated in the foregoing calculation to be ~4%. Figure 15 shows the comparison of the results by the zonal method with natural blocks to those composed from both results of the Li-glass and the NE-213 detectors taking into account the natural abundance of lithium isotopes. Because the measurement positions are different from each other and the ^7Li TPR shows smooth distribution, the NE-213 data are interpolated to the Li-glass data. The discussion of the void effect could explain why the composed TPR was slightly higher than the zonal TPR, but the difference was not large. Furthermore, one should note that a Monte Carlo transport code must use an estimator with a finite volume such as a track length estimator in which the reaction rate is averaged in the volume.

In the WCC experiment, the results of the on-line and the passive methods were also compared with each other, as shown in Fig. 11 for the ^7Li and ^6Li TPRs, respectively. One can see that both results agree very

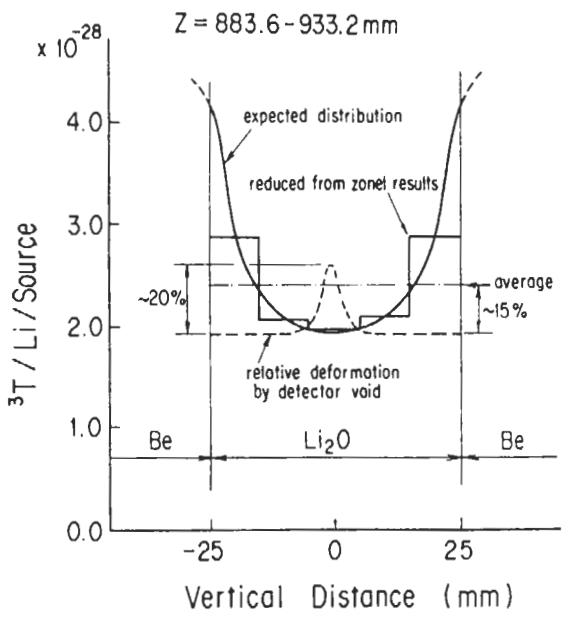

Fig. 14. Schematic illustration of the detector void effect on TPR measurement by the ^6Li-glass scintillator compared with the zonal measurement and the calculations.

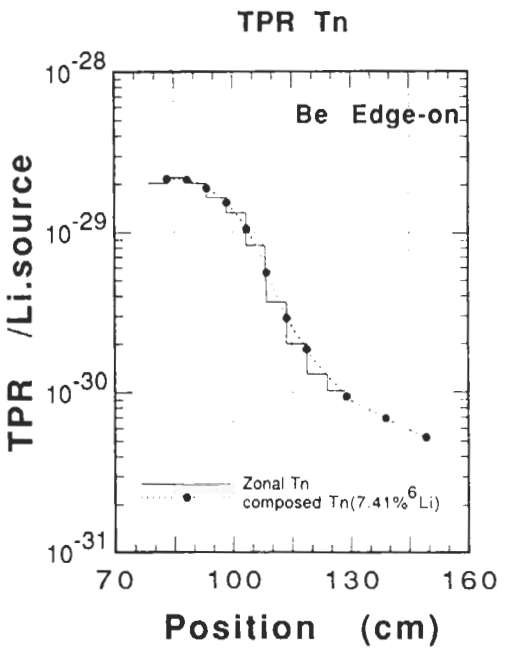

Fig. 15. Comparison of the tritium production from natural lithium measured by zonal blocks with the results composed of the ^7Li and the ^6Li TPR results obtained by the on-line methods. The natural abundance was assumed for the composition.

well as a whole. In this case, the void effect on the Li-glass result was expected to be small in contrast to the BEO case because the low-energy neutron flow was in the direction out of the coolant channel and the detector was attached to the front face of the void. For the ^{7}Li TPR, the NE-213 results were smaller than the Li-metal method. In this case, one should note that the NE-213 method was derived with the JENDL-3PR1 nuclear data of the ^{7}Li$(n,n'\alpha)$T reaction. Therefore, this indicates the underestimation of the JENDL-3PR1 cross section.

IV.C. Comparison with the Reference Blanket

The ratios of the current ^{7}Li TPR results obtained by the NE-213 indirect method to the data of the reference (REF) experiments[20] are shown in Fig. 16. The reference blanket had no heterogeneous region made of only Li_2O. The reference data were interpolated to take ratios of the others because those were mostly on a smooth curve. The WCC results were lower than the others by ~20% while the BEO was very similar to the REF in the Be/Li_2O mixed zone but 10% smaller at the back of the mixed zone. The former arose from the existence of 5-mm-thick stainless steel of the first wall. The latter was due to the decrease in the number of neutrons penetrating to the back of the Be/Li_2O mixed zone. This was caused by smaller penetration of high-energy neutrons at the back of the beryllium layer because the macroscopic total cross section of beryllium was ~20% larger than that of the Li_2O zone. Figure 17 shows the ratios of the ^{6}Li TPR by the Li-glass detector for both blankets. A large increase was observed for the BEO experiment in the region from the surface to a 300-mm depth where the multilayer of beryllium was located. This enhancement of low-energy neutron flux is four times larger than the REF experiment, which has no heterogeneous component. These low-energy neutrons were produced by a large moderation of neutrons in the adjacent beryllium layers. Local enhancement that was two times larger around the coolant channels also existed. The enhancements reached the region at 25 mm from the channel center while the boundary was at 3.2 mm.

By integrating the TPRs along the distribution, the index of the local TBR gain could be estimated for these configurations. Table VII shows the line-integrated TPR along the central axis with spline-fitting interpolation for both the NE-213 and the Li-glass results. The natural case was composed of both results with natural abundance. The integrated region was divided into the heterogeneous zone and the back zone of Li_2O. In the WCC blanket, the polyethylene zone was excluded in the integration. This integration can be directly related to the local TBR in a reactor blanket. As a whole, the ^{7}Li results always decreased, and the ^{6}Li results increased by moderating materials such as beryllium and polyethylene. One can see in Table VII that the BEO

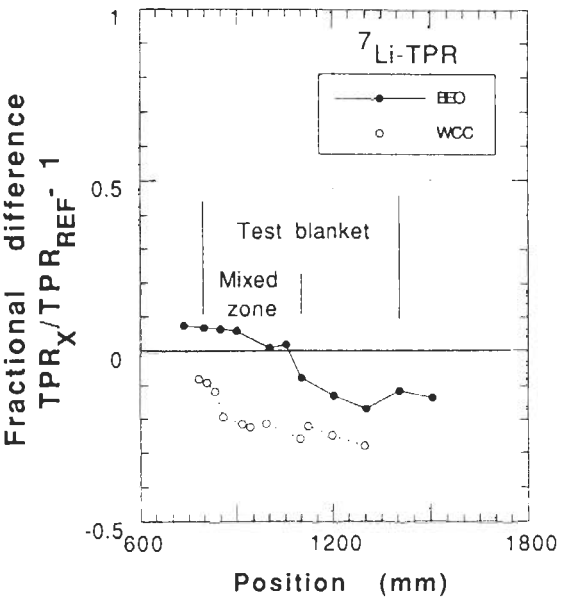

Fig. 16. Ratios of ^{7}Li TPR in the current test blankets to the homogeneous reference blanket.

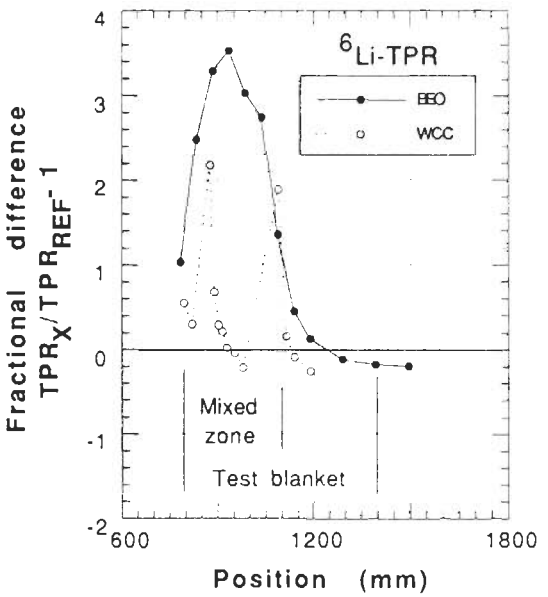

Fig. 17. Ratios of ^{6}Li TPR in the current test blankets to the homogeneous reference blanket.

blanket had a large TPR gain of 35% even with the volume fraction corrected value. Moreover, the water coolant much increased the TPR around the channel, and a local TBR gain reached ~30%, which was comparable to the BEO blanket. Though the content of the structure material, whose capture cross section competed with the ^{6}Li(n,α) reaction, was rather smaller

TABLE VII

Enhancement of Line-Integrated TPR (Ratio to the Reference) by Spline-Fitting Interpolation with TPR Distribution Data Measured by the On-Line Method

	BEO Blanket		WCC Blanket	
	Be/Li_2O Zone (790 to 1100 mm)	Back Zone (1100 to 1500 mm)	WCC Zone (800 to 1090 mm)	Back Zone (1090 to 1190 mm)
T_6	3.66 (1.83)[a]	1.21	1.55	1.07
T_7	1.05 (0.53)	0.88	0.81	0.76
T_n[b]	2.71 (1.36), 2.63[c]	1.16	1.28	1.01

[a]Parentheses denote the values corrected by 50% volume fraction of Li_2O zone.
[b]Values were composed of T_6 and T_7.
[c]Result by zonal method.

in this blanket, a TBR for the reactor blanket with a complicated cooling system should be carefully estimated because the heterogeneous effect is so delicate to calculate with a transport code. Table VII also shows that the integrated value of natural lithium measured by the zonal method agreed with the on-line method with 3% discrepancy.

IV.D. Comparison with Calculation

Because the shapes of the BEO assembly and the rotating target are three-dimensional, a Monte Carlo code suited a practical calculation analysis. The calculations shown in Fig. 8 with the measured in-system neutron spectra were obtained by the MORSE-DD neutron transport Monte Carlo code[21] with the JENDL-3PR1 nuclear data file.[22] This code was modified from the MORSE-CG code to use a double-differential form cross-section library with a 125-multigroup structure. This Monte Carlo calculation took ~11 h by using the FACOM 780 mainframe computer for the BEO experiment. Figure 8 indicates that the value of the measured flux in the 2- to 4-MeV range for the front measurement seems to be lower. This is possibly due to the spectrum distortion caused by a deficiency of the calculated neutron response used in spectrum unfolding, although the statistical error in the calculation was not enough in the 1- to 10-MeV range. Agreement between the measurement and the calculation was within 10 to 20% over the energy range in the measurement, except in the 1- to 10-MeV region. The calculations for the high-threshold reactions in the BEO blanket such as the $^{27}Al(n,\alpha)$ and the $^{7}Li(n,n'\alpha)$ reactions and the nonthreshold reaction of the $^{197}Au(n,\gamma)$ reaction are compared in Figs. 18 and 19, respectively. These calculated values were interpolated from the values of track detectors, which were defined as the same as zonal blocks. Figures 18 and 19 show that the calculations underestimated both high-threshold reactions by ~10% at the back zone of the test blanket. This trend was commonly found in comparison by MORSE-DD calculation for the reference blanket but not in calculation by a deterministic code[19] such as DOT3.5. This may suggest the possibility of a modeling uncertainty of the detector in a calculation. On the other hand, the calculated results of the $^{197}Au(n,\gamma)$ reaction agreed with the measurement within the statistical error, although it was very large. This also indicates that it is difficult for a Monte Carlo code to obtain a better estimation of the reaction rate for the case of a large cross section but a low neutron flux.

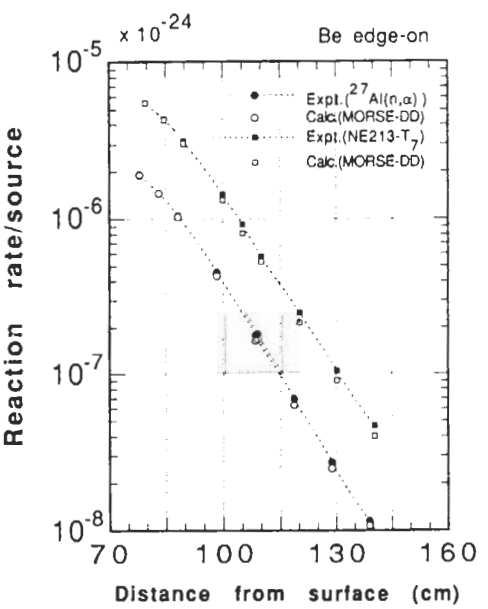

Fig. 18. Comparison of the measured high-threshold reactions with the MORSE-DD calculations in the BEO blanket.

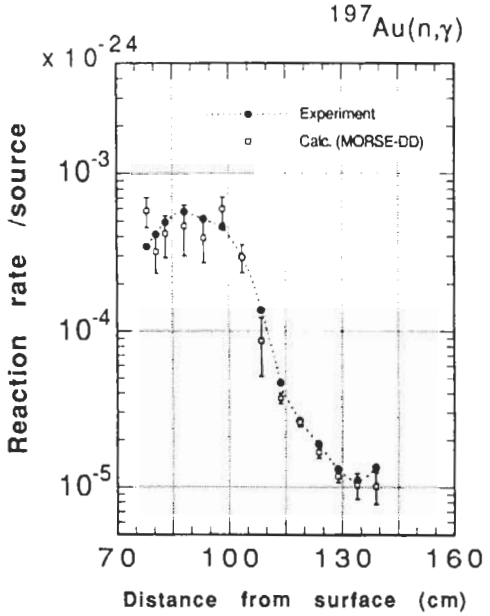

Fig. 19. Comparison of the measured $^{197}Au(n,\gamma)^{198}Au$ reaction with the MORSE-DD calculation in the BEO blanket.

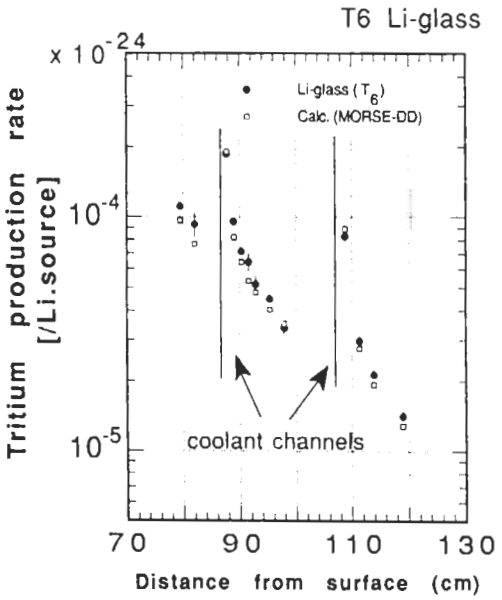

Fig. 20. Comparison of reaction rate around coolant channels between the measurement and the MORSE-DD calculation.

For the WCC test blanket, a comparison of the ^6Li TPR is shown in Fig. 20 for the Li-glass results. The calculation was carried out by track length estimators of thin plates that had 0.5-mm minimum thicknesses. The result was ~10% smaller than the measurement, especially in the first coolant channel region. This is the same trend as the BEO blanket but very different from the reference blanket where the calculation overestimated the ^6Li TPR by ~10%. In contrast, the high-threshold reactions showed the same tendency as the reference.

Consequently, the MORSE-DD calculation presented the neutron flux and reaction rates as having <10% discrepancies with the measurements. Detailed comparisons and discussions of the prediction accuracy of the different codes and the nuclear data are described in Ref. 5.

V. CONCLUSIONS

Nuclear parameters such as TPRs, neutron spectrum, and activation reaction rates were measured in fusion reactor–simulated blankets with heterogeneous configurations of the beryllium neutron multiplier and WCCs. The measured data had uncertainties ranging from 3 to 5% for the passive measurement methods and from 4 to 10% for the on-line methods. Several techniques were applied to the measurement of tritium production to play a complementary role. The comparison among the techniques clarified the effects depending on the method or the technical arrangement in a nonuniform neutron field around the heterogeneity. In these effects, the detector void effect was larger than the others especially for the ^6Li TPR measurement by the on-line detectors. In a neutron field of steep gradient, the zonal measurement was very accurate, but the spatial resolution was lost. On the other hand, the Li-foil method had good spatial resolution without the void effect, but it had lower efficiency and sometimes could fail because of tritium contamination. From the comparison between the test blankets, an enhancement of low-energy neutrons in the BEO zone and a change of neutron penetration behind it were observed. The TPR distribution significantly changed around the coolant channels, and its influence extended a distance of 25 mm from the channel. The MORSE-DD Monte Carlo code that used the previous version of JENDL-3 agreed with the experimental values to <10% accuracy but could not give enough statistical error for the low-energy response in a reasonable computing time.

Consequently, the MORSE-DD calculation agreed fairly with both experiments with <10% discrepancy. However, there were some difficulties at the material boundary in both the experimental and the calculation techniques. These should be improved by increasing neutron intensity and computing speed, respectively.

ACKNOWLEDGMENTS

We would like to express our appreciation to J. Kusano, C. Kutsukake, S. Tanaka, and Y. Abe for their excellent operation and maintenance of the neutron generator throughout this experiment. We would also like to thank S. Tamura

for his isotope dilution analysis of lithium of the Li_2O block and the Li-glass scintillator. The research in the United States was supported by the U.S. DOE Office of Fusion Energy.

REFERENCES

1. T. NAKAMURA and M. A. ABDOU, "Summary of Recent Results from the JAERI/U.S. Fusion Neutronics Phase I Experiments," *Fusion Technol.*, **10**, 541 (1986).

2. Y. OYAMA et al., "Measured Characteristics of Be Multi-Layered and Coolant Channel Blankets: Phase IIC Experiments of the JAERI/U.S. DOE Collaborative Program on Fusion Neutronics," *Fusion Technol.*, **19**, Part 2B, 1955 (1991).

3. Y. OYAMA et al., "Phase-IIC Experiments of the JAERI/U.S. DOE Collaborative Program on Fusion Blanket Neutronics, Volume I," JAERI-M 92-182, Japan Atomic Energy Research Institute (1992).

4. M. Z. YOUSSEF et al., "Phase-IIC Experiments of the JAERI/USDOE Collaborative Program on Fusion Blanket Neutronics, Volume II," UCLA-ENG-93-19, University of California, Los Angeles (1992).

5. M. Z. YOUSSEF et al., "Nuclear Analysis of Integral Experiments on a Li_2O Test Assembly with Local Heterogeneities Utilizing a 14-MeV Neutron Source," *Fusion Technol.*, **28**, 243 (1995) (in press).

6. M. NAKAGAWA et al., "Characteristics of a Deuterium-Tritium Fusion Source on a Rotating Target Used in Simulated Fusion Blanket Experiments," *Fusion Technol.*, **28**, 39 (1995); see also Y. OYAMA, Y. IKEDA, T. MORI, M. NAKAGAWA, T. NAKAMURA, and H. MAEKAWA, "Neutron Field Characteristics in a Concrete Cavity Having a DT Neutron Source," *Fusion Technol.*, **10**, 585 (1986).

7. H. MAEKAWA et al., "Neutron Yield Monitors for the Fusion Neutronics Source (FNS)," JAERI-M 83-219, Japan Atomic Energy Research Institute (1983).

8. A. KUMAR, Y. WATANABE, M. Z. YOUSSEF, and M. A. ABDOU, "Analysis for the Selection of Experimental Configurations for Heterogeneity and Be Multi-Layered Experiments of U.S.DOE/JAERI Collaborative Program on Blanket Neutronics," *Fusion Technol.*, **15**, Part 2B, 1309 (1989).

9. H. MAEKAWA et al., "Measured Neutron Parameters for Phase I Experiments at the FNS Facility," *Fusion Technol.*, **10**, 564 (1986).

10. Y. OYAMA et al., "Design and Techniques for Fusion Blanket Neutronics Experiments Using an Accelerator-Based Deuterium-Tritium Neutron Source," *Fusion Technol.*, **28**, 56 (1995).

11. K. G. PORGES and M. M. BRETSCHER, "Breeding Rate Measurements in Solid Fusion Blankets with Metallic Lithium Samples," *Fusion Technol.*, **19**, 1903 (1991).

12. K. TSUDA, Japan Atomic Energy Research Institute, Private Communication (1985).

13. S. YAMAGUCHI, Y. OYAMA, T. NAKAMURA, and H. MAEKAWA, "An On-Line Method for Tritium Production Measurement with a Pair of Lithium-Glass Scintillators," *Nucl. Instrum. Methods*, **A254**, 413 (1987).

14. S. CHIBA and K. SHIBATA, "Revision and Status of the Neutron Nuclear Data of ^{6}Li and ^{7}Li," JAERI-M 88-164, Japan Atomic Energy Research Institute (1988).

15. Y. OYAMA, S. TANAKA, K. TSUDA, Y. IKEDA, and H. MAEKAWA, "A Small Spherical NE213 Scintillation Detector for Use in In-Assembly Fast Neutron Spectrum Measurements," *Nucl. Instrum. Methods*, **A256**, 333 (1987).

16. "FORIST Spectra Unfolding Code," PSR-92, Radiation Shielding Information Center, Oak Ridge National Laboratory (1975).

17. E. F. BENNETT and T. J. YULE, "Response Functions for Proton-Recoil Proportional Counter Spectrometer," *Nucl. Instrum. Methods*, **98**, 333 (1972).

18. Y. IKEDA et al., "Activation Cross Section Measurements for Fusion Reactor Structural Materials at Neutron Energy from 13.3 to 15.0 MeV Using FNS Facility," JAERI 1312, Japan Atomic Energy Research Institute (1988).

19. W. A. RHOADES and F. R. MYNETT, "The DOT III Two Dimensional Discrete Ordinates Transport Code," ORNL-TM-4280, Oak Ridge National Laboratory (1973).

20. C. KONNO et al., "Neutronics Integral Experiments of Simulated Fusion Reactor Blanket with Various Beryllium Configurations for Deuterium-Tritium Neutrons," *Fusion Technol.*, **28** (Sep. 1995); see also Y. OYAMA et al., "Phase-IIA and IIB Experiments of JAERI/USDOE Collaborative Program on Fusion Blanket Neutronics," JAERI-M 89-215, Japan Atomic Energy Research Institute (1989).

21. M. NAKAGAWA and T. MORI, "MORSE-DD, A Monte Carlo Code Using Double Differential Form Cross Sections," JAERI-M 84-126, Japan Atomic Energy Research Institute (1984).

22. K. SHIBATA, "Evaluation of Neutron Nuclear Data of ^{6}Li, ^{7}Li and ^{9}Be for JENDL-3," JAERI-M 84-198, 84-204, and 84-226, Japan Atomic Energy Research Institute (1984).

Yukio Oyama (BS, physics, 1975; MS, nuclear physics, 1977; and Dr. Eng., 1989, Osaka University, Japan) is a principal scientist at the Japan Atomic

Energy Research Institute (JAERI). He has worked in the area of fusion neutronics experiments since 1978. He is currently involved in intense and high-energy neutron source projects.

Chikara Konno (MS, physics, Kyoto University, Japan, 1985) is a research scientist in the Department of Reactor Engineering at JAERI. He has worked in the areas of fusion neutronics experiments, cross-section measurements, and neutron spectrum measurements using a proton-recoil counter.

Yujiro Ikeda (PhD, nuclear engineering, Nagoya University, Japan, 1981) is head of the Fusion Neutronics Laboratory in the Department of Reactor Engineering at JAERI. He has worked in the areas of fusion neutronics experiments, induced radioactivity experiment and analysis, direct nuclear heating measurements, activation cross-section measurements, and fusion dosimetry.

Seiya Yamaguchi (BS, applied physics, Waseda University, Japan, 1980; MS, 1982, and PhD, 1989, energy sciences, Tokyo Institute of Technology, Japan) in 1982 joined the Department of Reactor Engineering at JAERI, where he engaged in research and development on the design and characterization of Li-glass scintillator for fusion neutronics application. From 1989, he was a research assistant with Photon Factory at KEK, National Laboratory for High Energy Physics, where he worked in the areas of microwave engineering for the electron linear accelerator.

Koichi Tsuda (BS, nuclear engineering, University of Tokyo, Japan, 1982) is a research scientist at JAERI. He has worked in the area of fusion neutronics experiments since 1982. He is especially involved in tritium measurement.

Kazuaki Kosako (BE, atomic engineering, Tokai University, Japan, 1984) has worked at Sumitomo Atomic Energy Industries since 1994. He worked in the Department of Reactor Engineering at JAERI from 1984 to 1992 where he was involved mainly in fusion neutronics. He is currently interested in the area of radiation damage of materials.

Hiroshi Maekawa (BE, 1965; MS, 1967; and Dr. Eng., 1970, nuclear engineering, Tokyo Institute of Technology, Japan) is the deputy director of the Department of Reactor Engineering and the head of the Intense Neutron Source Laboratory at JAERI. He has worked on fusion neutronics for more than 20 years, and he planned and constructed the Fusion Neutronics Source (FNS) facility. He served as the Japanese leader of the JAERI/U.S. Department of Energy (U.S. DOE) collaboration on fusion blanket neutronics. His recent research has focused on International Fusion Materials Irradiation Facility conceptual design activities.

Masayuki Nakagawa (BS, 1965; MS, 1967; and PhD, 1979, nuclear engineering, Kyoto University, Japan) is a principal scientist in the Department of Reactor Engineering at JAERI. He is a head of the reactor system laboratory having the main responsibility for the computation method and design of reactors. He researched the development of neutronics computation methods and codes for fast reactors and fusion reactors and intelligent reactor design systems. His group has developed high-speed general-purpose Monte Carlo codes based on vector and/or parallel algorithms.

Takamasa Mori (BS, 1976; MS, 1979; and PhD, 1985, nuclear engineering, Kyoto University, Japan) is a principal scientist in the Department of Reactor Engineering at JAERI. He worked for the development of neutron transport codes using double-differential from cross sections. His research interests are in the field of reactor physics, especially the speedup of Monte Carlo calculation of high-energy particles based on vector and/or parallel algorithms.

Tomoo Nakamura (BS, physics, Kyoto University, Japan, 1957) is currently director of the Public Acceptance Database Center, Research Organization for Information Science and Technology. His research background includes experimental reactor physics on fast breeder reactors and nuclear technology on fusion reactor blankets. He served as the former Japanese leader of the JAERI/U.S. DOE collaboration on fusion blanket neutronics.